RSC Advances

PAPER

View Article Online
View Journal | View Issue

Check for updates

Cite this: *RSC Adv.*, 2017, 7, 44626

$CdS-MoS_2$ heterostructures on Mo substrates *via in situ* sulfurization for efficient photoelectrochemical hydrogen generation†

Xianglin Zhu,[a] Peng Wang,*[a] Qianqian Zhang,[a] Zeyan Wang,[a] Yuanyuan Liu,[a] Xiaoyan Qin,[a] Xiaoyang Zhang,[a] Ying Dai[b] and Baibiao Huang*[a]

Received 6th June 2017
Accepted 31st August 2017

DOI: 10.1039/c7ra06304k

rsc.li/rsc-advances

A $CdS-MoS_2$ photoelectrode with a double-layer core–shell structure was prepared using a simple electrodeposition–*in situ* sulfurization method on a Mo substrate. The photocatalytic activity of as-prepared electrodes was evaluated using a photoelectrochemical H_2-generation experiment. The photocurrent and photon–electron conversion efficiency of the $CdS-MoS_2$ photoelectrode were nearly double those of a CdS photoanode prepared on FTO glass. The high activity of the $CdS-MoS_2$ photoelectrode was due to the higher separation efficiency of carriers caused by the formed $CdS-MoS_2$ Janus heterojunction structure, which made directional transmission and electron–hole separation possible. Our experiments show that, in addition to being a good co-catalyst in powder material for photocatalytic hydrogen production, MoS_2 can also be used as an electron acceptor layer to enhance electron–hole separation.

1. Introduction

The development of modern society has been built on energy consumption, with large amounts of fossil fuels, including coal, oil, and natural gas, burned to power the fast development of the world economy over the last hundred years. However, these fossil fuels are nonrenewable and cause environmental damage. Environmental problems caused by burning fossil fuels have attracted global attention. An ideal energy source to replace fossil fuels would be an effective solution for energy and environmental problems. Solar energy is abundant and clean, making it an excellent candidate. Solar energy conversion has become a hot topic in recent years.[1–12] Storing solar energy in the form of hydrogen energy using photoelectrochemical (PEC) water splitting technology is considered a promising solution to provide ample clean energy to satisfy the increasing demands of modern society.[13,14]

In harnessing solar energy to split water with the necessary efficiency, the most important factors are light capture and carrier separation. Some n-type semiconductor photoanodes have shown the ability to split water at low over-potentials, such as TiO_2, ZnO, and WO_3, and their applications in PEC water splitting have received much attention. Due to self-defects, these materials can only absorb pure UV light or have poor stabilities under sunlight irradiation,[15–21] greatly limiting the use of solar energy. Accordingly, developing photoanodes with narrow band gaps that can absorb and utilize visible light is essential to enhance photoelectric water splitting efficiency. CdS, a well-known semiconductor material for PEC water splitting, has outstanding potential due to its excellent visible light absorption properties. The activity of CdS photoanodes is mainly limited by the efficiency of photogenerated carrier separation. Several types of CdS-based photoelectrodes have been developed with high efficiency in PEC hydrogen production, including CdS/TiO_2, CdS/ZnO, and CdS/ZnS.[22–24] However, preparation of these structures is usually complicated, with the facile construction of CdS photoanodes with high activity remaining a challenge. Among various exploratory approaches to the promotion of carrier transport and separation, constructing a core–shell structure has been shown to be especially advantageous for promoting carrier separation and improving stability owing to the separation of reduction and oxidation sites.[25–32]

Herein, we have synthesized CdS photoanodes on a Mo mesh substrate using an electrodeposition sulfurization method, which produces a layer of MoS_2 between CdS and Mo metal during sulfurization. Experiments showed that the generated CdS and MoS_2 layers formed a double-layer shell around an Mo core. Furthermore, the CdS and MoS_2 layers formed a special CdS/MoS_2 Janus heterojunction that was able to promote the directional transmission of photogenerated electrons and enhance photocatalytic performance.

[a]State Key Laboratory of Crystal Materials, Shandong University, Jinan 250100, China. E-mail: pengwangicm@sdu.edu.cn; bbhuang@sdu.edu.cn; Fax: +86-0531-88365969; Tel: +86-0531-88366139

[b]School of Physics, Shandong University, Jinan 250100, China

† Electronic supplementary information (ESI) available. See DOI: 10.1039/c7ra06304k

2. Experimental sections

2.1. Materials and reagents

All reagents used in experiments, including $CdCl_2$, Na_2SO_4, Na_2SO_3, and Na_2S, were purchased from Aladdin reagent and used without further purification. Mo mesh (99.9%) was soaked in 20% hydrochloric acid for 24 h, and then cleaned ultrasonically with deionized water, ethanol, and acetone for 20 min before use.

2.2. Preparation of CdS–MoS_2 photoelectrodes

CdS–MoS_2 photoelectrodes were prepared using an electrodeposition-sulfurization method. Firstly, Cd metal was electroplated onto Mo mesh in 20 mM $CdCl_2$ solution at a bias voltage of −1.0 V using a three-electrode system comprising a platinum plate counter electrode and saturated Ag/AgCl reference electrode. Different amounts of Cd were deposited by adjusting the deposition time and deposition charge, (0.5 C, 1.0 C, 2.0 C, 3.0 C, and 5.0 C). The prepared electrodes were denoted CdS–MoS_2-x, where x is the deposition charge. The deposition current was about 3 mA and two-thirds of the Mo mesh was kept submerged in the solution throughout the process. The deposited electrode was dried with pure N_2. The Mo mesh was then sulfurized under an H_2S atmosphere by heating to 500 °C at a rate of 10 °C min^{-1} and then holding at 500 °C for 1 h. Pure N_2 was used to purge remaining H_2S during cooling. During sulfurization, some Mo also reacted with H_2S gas, producing a layer of MoS_2 between the Mo core and CdS shell.

For comparison, CdS photoelectrodes without the MoS_2 layer were prepared on a fluorine-doped tin oxide (FTO) glass substrate, as the Cd layer was too thin to prevent MoS_2 generation when using Mo metal as substrate. Typically, CdS/FTO photoelectrodes were prepared according to a literature method,[36] but with the reaction time increased to 10 h to achieve the best photoelectric properties.

2.3. Characterization

The structure of the CdS–MoS_2 photoelectrode was characterized by X-ray diffraction (XRD) on a Bruker AXS D8 advance powder diffractometer (Cu Kα X-ray radiation, $\lambda = 0.154\,056$ nm). The morphology of the as-prepared photoelectrodes was obtained using scanning electron microscopy (SEM, Hitachi S4800). The light source was a 300 W Xe arc lamp (PLS-SXE 300, Beijing Trusttech Co. Ltd.) equipped with an AM 1.5 filter. The amount of H_2 produced was determined by gas chromatography (GC, Varian GC-3800) equipped with a thermal conductivity detector.

2.4. Electrochemical measurements

The photoelectrochemical activity of CdS photoelectrodes was evaluated in a quartz cell using a three-electrode system based on a Chenghua electrochemical work station (CHI660C, Shanghai). A Pt plate and commercially available Ag/AgCl electrode were used as the counter electrode and reference electrode, respectively, with the prepared CdS photoelectrode used as the working electrode. The electrolyte used in all measurements was an aqueous solution containing 0.1 M Na_2SO_4, 0.05 M Na_2S, and 0.05 M Na_2SO_3 at pH 12.6.

3. Results and discussion

The phase and composition of the CdS–MoS_2 photoelectrode were investigated, with Fig. 1 showing the X-ray diffraction (XRD) patterns of CdS–MoS_2. The blue line is the pattern for CdS–MoS_2, while red and black lines correspond to the standard cards of hexagonal phase CdS and Mo metal, respectively. The XRD results show that the prepared CdS was pure hexagonal phase with good crystallinity. Typically, photocatalytic activity is closely correlated with photocatalyst crystallinity, with good crystallinity usually benefitting the photocatalytic reaction. No obvious MoS_2 peaks could be distinguished, meaning that very little MoS_2 was formed during the reaction.

The surface morphology of the CdS–MoS_2 photoelectrode was characterized by SEM. Fig. 2(a–d) show images of the CdS–MoS_2 photoelectrode before the photocatalytic experiment. As shown in Fig. 2(a) and (b), CdS was generated on the surface of MoS_2 and the Mo mesh with uniform morphology. The magnified SEM images (Fig. 2(c) and (d)) showed plate-like CdS with heights of about 1.2 μm (Fig. S1b†) embedded uniformly in the surface. This plate-like CdS can increase the reaction area, which improves photoelectric activity. Fig. 2(e) and (f) show surface images of CdS after the photocatalytic experiment. The surface of plate-like CdS became rough, perhaps due to photocorrosion.

To further investigate the internal composition and structure of CdS–MoS_2 samples, the electrodes were immersed in 1 M HCl solution for 30 min (CdS can react with dilute hydrochloric acid, $CdS + HCl \rightarrow H_2S\uparrow + CdCl_2$, while MoS_2 is more stable in dilute hydrochloric acid solution) to remove surface CdS. The surface elemental composition before and after treatment with HCl solution was analyzed by EDS mapping (Fig. 3(a–e)). The results before HCl treatment confirmed the uniform distribution of Cd and S, with no Mo element detected. This indicated that the CdS layer was compact and could fully cover the electrode surface.

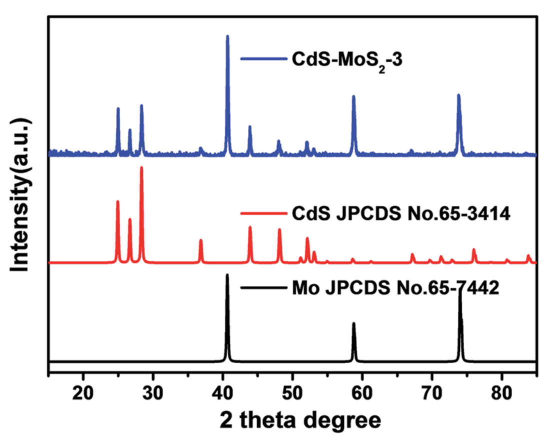

Fig. 1 XRD pattern of CdS–MoS_2-3 photoelectrode in comparison with CdS and Mo standards.

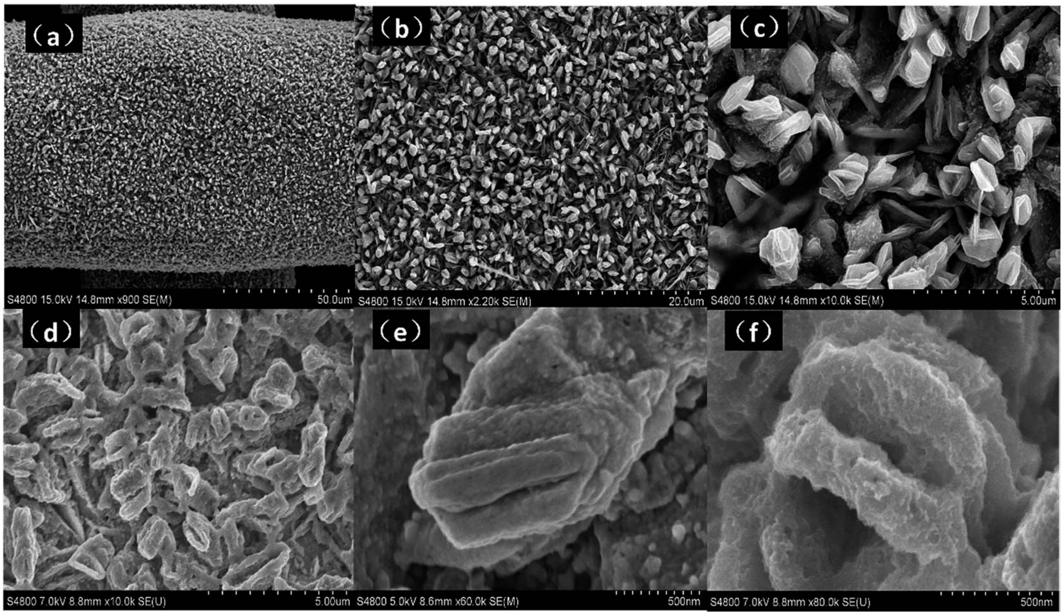

Fig. 2 SEM images of CdS–MoS_2 electrode (a–d) before and (e, f) after the photocatalytic test.

The mapping results after treatment with HCl solution showed that only a small amount of elemental Cd existed and that its distribution was uneven, while Mo and S remained uniformly distributed. From the above EDS mapping characterizations, it was concluded that a Mo–S compound was generated under the CdS layer.

The electrodes before and after HCl solution treatment were analyzed by X-ray photoelectron spectroscopy (XPS). Cd 3d, Mo 3d, and S 2p spectra are shown in Fig. 4. The spectra of untreated samples showed characteristic Cd 3d, S 2s, and S 2p peaks, but no elemental Mo peaks were found. After treatment with HCl solution, the XPS results were very different. The intensity of the Cd 3d peaks became weaker, with only one Cd $3d_{3/2}$ peak distinguishable at 412.1 eV. Another characteristic peak at around 405.3 eV was not clearly observed. The XPS of Cd also showed that most elemental Cd was removed by HCl solution. The Mo 3d XPS spectra were resolved into four peaks at around 231.6 eV and 228.5 eV that were assigned to Mo^{4+} $3d_{3/2}$ and Mo^{4+} $3d_{5/2}$, respectively.[34] The S 2p XPS spectra were resolved into three peaks, corresponding to two components. Peaks at 162.7 eV and 161.5 eV were attributed to S $2p_{3/2}$ and S $2p_{1/2}$ signals in MoS_2, while the peak at around 164.0 eV was attributed to bridging disulfides, S_2^{2-}, which have been reported previously[35] XPS of Mo and S indicated that MoS_2 was formed beneath the CdS layer. Notably, Mo^0 was not detected by XPS, proving that the Mo^0 core was completed covered with a MoS_2 layer.

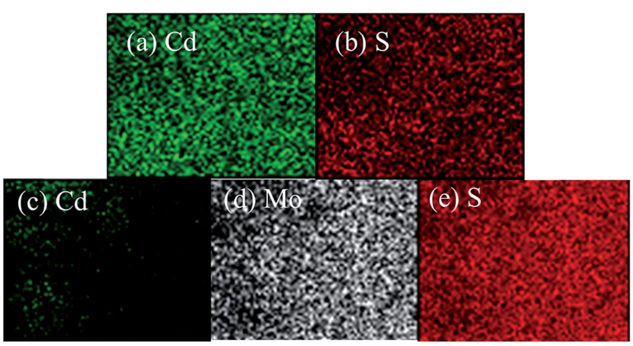

Fig. 3 EDS element mapping results of the CdS–MoS_2 electrode (a, b) before and (c–e) after treating with HCl solution.

From the XPS and EDS results, we concluded that the prepared CdS–MoS_2 electrodes contained a CdS–MoS_2–Mo double-layer core–shell structure. To understand the interactions of CdS and MoS_2, Mott–Schottky plots of CdS/MoS_2 and CdS/FTO photoanodes were produced, as shown in Fig. S4.† These plots showed that the flat band potential of CdS shifted toward high voltage for the existing of MoS_2 layer, indicating heterojunction formation.[37,38] In such a structure, the CdS and MoS_2 layers construct a CdS/MoS_2 type-I heterojunction with a Janus structure. Therefore, photogenerated electrons in the CdS layer are likely transferred to the MoS_2 layer under visible light irradiation, while holes remain in the CdS layer, resulting in the separation of photogenerated electrons and holes. This type of CdS/MoS_2 Janus structure is advantageous for the directional transmission of carriers and enhances photoelectric activity.[33] In the CdS/FTO photoanodes, CdS contacted with FTO directly and there was no forced directional transmission of the photogenerated carriers. Therefore, the CdS/FTO photoanodes showed weaker activity than the prepared CdS–MoS_2 photoelectrodes.

To further examine the activity of CdS–MoS_2 photoelectrodes in PEC cells, electrochemical experiments were performed using a three-electrode system. Fig. 5(a) shows current–potential curves of the as-prepared CdS–MoS_2 photoelectrodes and CdS/FTO photoelectrodes. Linear sweep voltammograms of the

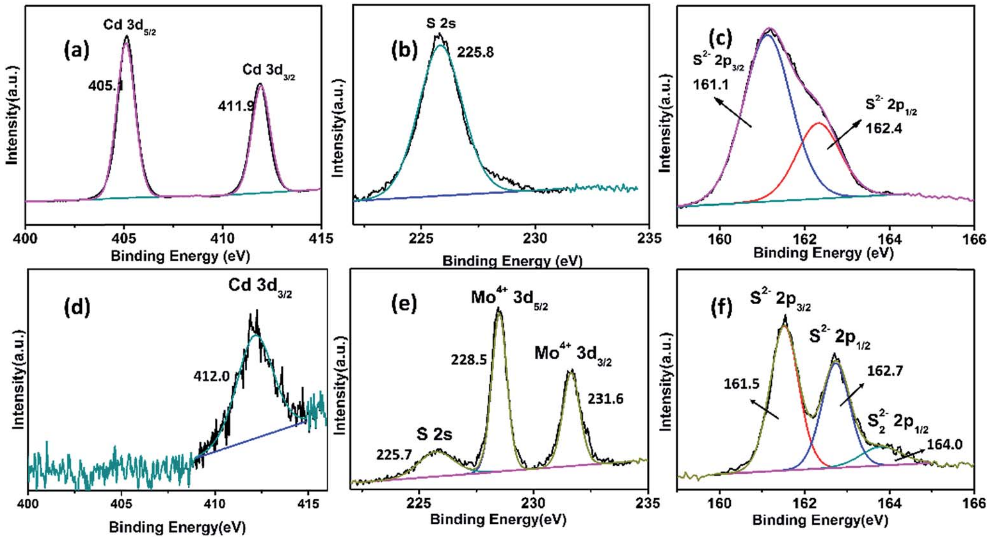

Fig. 4 XPS spectra of electrode (a–c) before and (d–f) after treatment with HCl solution.

electrodes were recorded under light illumination and in the dark intermittently at a rate of 5 mV s^{-1}. The results show that activity was affected by deposition amount. When the deposition electric charge was 0.5 C or 1.0 C, the prepared CdS–MoS_2 photoelectrodes showed poor activity. Furthermore, the dark current was very high during experiments, proving that electric leakage was occurring. CdS–MoS_2-3 and CdS–MoS_2-5 showed good photoelectric activities, while CdS–MoS_2-3 showed the better performance. The deposition amount also influenced the initial potential, with higher deposition amounts corresponding to lower initial potentials. For comparison, the linear sweep voltammogram results of the CdS/FTO electrode were also characterized, as shown in Fig. 5(a). The results show that the prepared CdS/FTO photoelectrode had good photoelectric activity, but worse than that of CdS–MoS_2-3 and CdS–MoS_2-5. Considering the photoelectric activity and initial potential, a deposition amount of 3C was deemed the most appropriate.

Fig. 5(b) and (c) show *I–t* curves of photoelectrodes at a potential of 0.9 V *vs.* RHE. The stable light current density of CdS–MoS_2-3 was about 3.5 mA cm^{-2}, while that of CdS/FTO was about 1.7 mA cm^{-2}. During the experiment, CdS/FTO showed good stability, while the light current density of CdS–MoS_2-3 decreased to 3.5 mA cm^{-2} from 4.0 mA cm^{-2} in 600 s. The cycling experiment of CdS–MoS_2-3 after electrolyte replication,

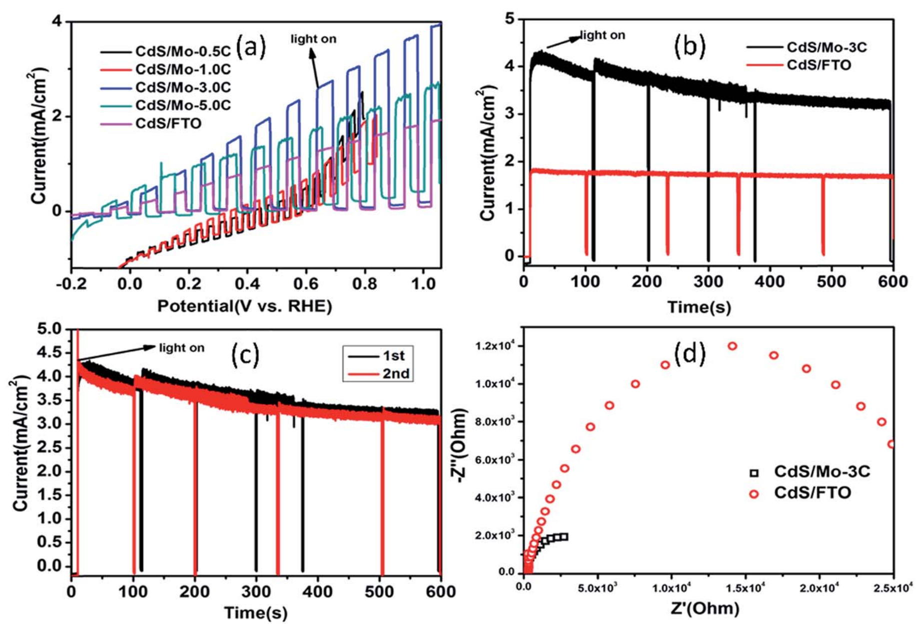

Fig. 5 Photoelectrochemical measurements. (a) Current–potential curves of as-prepared CdS–MoS_2 and CdS/FTO photoelectrodes. (b) Light current densities of CdS–MoS_2 and CdS/FTO electrodes. (c) Cycling experiment of CdS–MoS_2. (d) Nyquist plot of CdS electrodes.

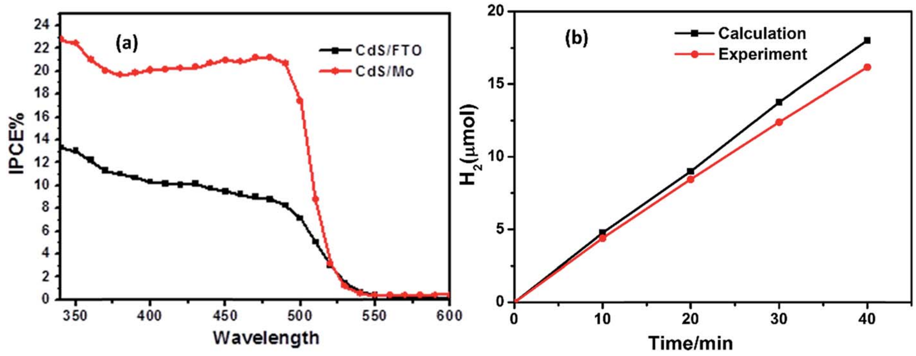

Fig. 6 IPCE and photoelectric H_2 production experiment.

as shown in Fig. 5(c), showed no obvious change in activity in the second test, demonstrating that the CdS–MoS_2-3 photoelectrode had good stability in the photoelectric test. EDS analysis (Fig. S2†) showed that the ratio of S and Cd elements after photocatalytic reaction was larger than that before the test. This indicated that the decrease of photoactivity was due to sulfur deposition during the reaction caused by oxidation of S^{2-}.

Efficient charge transfer was further verified by electrochemical impedance spectra (EIS).[33] Fig. 5(d) shows EIS results for CdS–MoS_2-3 and CdS/FTO photoelectrodes under UV-visible light irradiation. The results show that the EIS curve diameter for CdS–MoS_2-3 was smaller than that of CdS/FTO, with a smaller radius diameter corresponding to smaller charge-transfer resistance in the EIS Nyquist plot, better electroconductivity, and faster separation efficiency of photogenerated electron–hole pairs on the Cd/Mo electrodes compared with the CdS/FTO sample.

Incident photon-to-electron conversion efficiency (IPCE) is an important index for evaluating photoelectrode activity, and was characterized, as shown in Fig. 6(a). The black and red lines correspond to the IPCE results of the CdS/FTO electrode and the CdS–MoS_2-3 electrode, respectively. The IPCE of the CdS–MoS_2-3 electrode was higher than that of the CdS/FTO electrode. Furthermore, the IPCE of the CdS–MoS_2-3 electrode in the wavelength range 420–500 nm was more than twice that of the CdS/FTO electrode. The IPCE results showed that CdS–MoS_2 on the Mo substrate could convert more solar energy than that on FTO glass. The faradaic efficiency was calculated using a photoelectric water splitting experiment. The graph in Fig. 6(b) shows that H_2 generation was good and linear, and that the faradaic efficiency of the CdS–MoS_2-3 photoelectrode was over 90%.

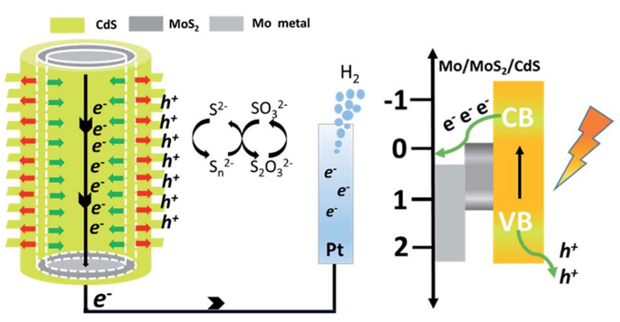

Fig. 7 Schematic diagram of structure and carrier separation.

Based on the above experiments and characterization results, we have proposed a possible mechanism to explain the better performance of CdS–MoS_2 photoelectrodes compared with the CdS/FTO electrode, as shown in Fig. 7. During Cd sulfurization, some Mo metal reacts with H_2S, forming a MoS_2 layer between CdS and the Mo substrate. On the CdS anode, photogenerated holes are captured by S^{2-}, while electrons are more likely to migrate to the counter electrode and generate H_2. The formed CdS/MoS_2 Janus heterojunction takes advantage of the separation of photogenerated electrons and holes along the given direction, which can enhance the carrier separation efficiency. As a result, the prepared CdS–MoS_2 structure showed high photoelectric activity.

4. Conclusion

In summary, efficient CdS–MoS_2 photoelectrodes were prepared using a simple electrodeposition-sulfurization method. The CdS–MoS_2 photoelectrodes had higher activities in photoelectric water splitting than CdS/FTO electrodes. EDS and XPS characterization indicated that the prepared electrodes had a unique CdS–MoS_2–Mo double-layer core–shell structure. The presence of a Janus CdS/MoS_2 heterojunction was favorable for directional transmission and electron–hole separation. Therefore, the CdS–MoS_2 photoelectrodes showed improved activity. These results confirm that, in addition to being a good co-catalyst in powder materials for photocatalytic hydrogen production, MoS_2 can enhance the separation efficiency of photoelectrodes by forming a heterojunction. The preparation of these CdS–MoS_2 photoanodes will aid the further design of highly efficient photoanodes.

Conflicts of interest

There are no conflicts to declare.

Acknowledgements

This work is financially supported by the National Basic Research Program of China (the 973 program, 2013CB632401), the National Natural Science Foundation of China (21333006, 21573135, 11374190, 51602179, and 51321091). P. Wang acknowledges support from The Recruitment Program of Global Experts, China. B. B. H. acknowledges support from the Taishan Scholars Program of Shandong Province.

References

1 K. Sekizawa, K. Maeda, K. Domen, K. Koike and O. Ishitani, *J. Am. Chem. Soc.*, 2013, **135**, 4596–4599.
2 J. G. Yu, J. X. Low, W. Xiao, P. Zhou and M. Jaroniec, *J. Am. Chem. Soc.*, 2014, **136**, 8839–8842.
3 X. Zong, H. J. Yan, G. P. Wu, G. J. Ma, F. Y. Wen, L. Wang and C. Li, *J. Am. Chem. Soc.*, 2008, **130**, 7176–7177.
4 Q. Li, B. D. Guo, J. G. Yu, J. R. Ran, B. H. Zhang, H. J. Yan and J. R. Gong, *J. Am. Chem. Soc.*, 2011, **133**, 10878–10884.
5 Q. L. Tay, X. H. Wang, X. Zhao, J. D. Hong, Q. Zhang, R. Xu and Z. Chen, *J. Catal.*, 2016, **342**, 55–62.
6 T. Kamegawa, H. Seto, S. Matsuura and H. Yamashita, *ACS Appl. Mater. Interfaces*, 2012, **4**, 6635–6639.
7 X. L. Zhu, P. Wang, B. B. Huang, X. C. Ma, X. Y. Qin, X. Y. Zhang and Y. Dai, *Appl. Catal., B*, 2016, **199**, 315–322.
8 W. Z. Zhong, T. Qiao, J. Dai, L. Q. Mao, Q. Xu, G. Q. Zou, X. X. Liu, D. L. Yin and F. P. Zhao, *J. Catal.*, 2015, **330**, 208–221.
9 M. Navlani-García, K. Mori, A. Nozaki, Y. Kuwahara and H. Yamashita, *Ind. Eng. Chem. Res.*, 2016, **55**, 7612–7620.
10 S. S. Chen, Y. Qi, Q. Ding, Z. Li, J. Y. Cui, F. X. Zhang and C. Li, *J. Catal.*, 2016, **339**, 77–83.
11 Z. K. Zheng, T. Tachikawa and T. Majima, *J. Am. Chem. Soc.*, 2014, **136**, 6870–6873.
12 Q. J. Xiang, J. G. Yu and M. Jaroniec, *J. Am. Chem. Soc.*, 2012, **134**, 6575–6578.
13 A. Fujishima and K. Honda, *Nature*, 1972, **238**, 37–38.
14 W. Q. Fan, C. Chen, H. Y. Bai, B. F. Luo, H. Q. Shen and W. D. Shi, *Appl. Catal., B*, 2016, **195**, 9–15.
15 J. H. Han, Z. F. Liu, K. Y. Guo, X. Q. Zhang, T. T. Hong and B. Wang, *Appl. Catal., B*, 2015, **179**, 61–68.
16 L. P. Wu, Y. L. Zhang, L. Z. Long, C. P. Cen and X. J. Li, *RSC Adv.*, 2014, **4**, 20716.
17 M. Kodera, H. Urabe, M. Katayama, T. Hisatomi, T. Minegishi and K. Domen, *J. Mater. Chem. A*, 2016, **4**, 7658–7664.
18 C. Fàbrega, S. Murcia-López, D. Monllor-Satoca, J. D. Prades, M. D. Hernández-Alonso, G. Penelas, J. R. Morante and T. Andreu, *Appl. Catal., B*, 2016, **189**, 133–140.
19 R. Lv, T. Wang, F. L. Su, P. Zhang, C. J. Li and J. L. Gong, *Nano Energy*, 2014, **7**, 143–150.
20 G. M. Wang, H. Y. Wang, Y. C. Ling, Y. C. Tang, X. Y. Yang, R. C. Fitzmorris, C. C. Wang, J. Z. Zhang and Y. Li, *Nano Lett.*, 2011, **11**, 3026–3033.
21 S. C. Wang, H. J. Chen, G. P. Gao, T. Butburee, M. Q. Lyu, S. Thaweesak, J.-H. Yun, A. Du, G. Liu and L. Z. Wang, *Nano Energy*, 2016, **24**, 94–102.
22 J. Zhang, L. H. Wang, X. H. Liu, X. A. Li and W. Huang, *J. Mater. Chem. A*, 2015, **3**, 535–541.
23 B. K. Liu, Y. F. Xue, J. T. Zhang, D. J. Wang, T. F. Xie, X. Y. Suo, L. L. Mu and H. Z. Shi, *Electrochim. Acta*, 2016, **19**, 370–376.
24 H. Li, C. Z. Yao, L. X. Meng, H. Sun, J. Huang and Q. J. Gong, *Electrochim. Acta*, 2013, **108**, 45–50.
25 Y. F. Tang, X. L. Liu, C. C. Ma, M. J. Zhou, P. W. Huo, L. B. Yu, J. M. Pan, W. D. Shi and Y. S. Yan, *New J. Chem.*, 2015, **39**, 5150–5160.
26 E. Ha, L. Y. S. Lee, H.-W. Man, S. C. E. Tsang and K.-Y. Wong, *ACS Appl. Mater. Interfaces*, 2015, **7**, 9072–9077.
27 W. W. Xu, Z. Q. Xie, Z. Wang, G. Dietrich and Y. Wang, *J. Mater. Chem. A*, 2016, **4**, 19011–19018.
28 Y. N. Tang, W. H. Di, X. S. Zhai, R. Y. Yang and W. P. Qin, *ACS Catal.*, 2013, **3**, 405–412.
29 J. K. Zhang, Z. B. Yu, Z. Gao, H. B. Ge, S. C. Zhao, C. Q. Chen, S. A. Chen, X. L. Tong, M. H. Wang, Z. F. Zheng and Y. Qin, *Angew. Chem., Int. Ed.*, 2016, **55**, 1–6.
30 J. Y. Zhang, Y. H. Wang, J. Jin, J. Zhang, Z. Lin, F. Huang and J. G. Yu, *ACS Appl. Mater. Interfaces*, 2013, **5**, 10317–10324.
31 Y. Zhu, Y. J. Wang, Q. Ling and Y. F. Zhu, *Appl. Catal., B*, 2017, **200**, 222–229.
32 F. Liu, W. Q. Yao, D. Liu, R. L. Zong, M. Zhang, X. G. Ma and Y. F. Zhu, *Appl. Catal., B*, 2015, **163**, 547–553.
33 P. Wu, C. G. Tian, Y. Q. Jiao, Q. Yan, G. Y. Yang and H. G. Fu, *Appl. Catal., B*, 2017, **203**, 955–963.
34 Y. Liu, Y.-X. Yu and W.-D. Zhang, *J. Phys. Chem. C*, 2013, **117**, 12949–12957.
35 H. Vrubel, D. Merki and X. Hu, *Energy Environ. Sci.*, 2012, **5**, 6136–6144.
36 G. Bao, C. F. Wang, L. Dong, C. Y. Shen, K. Zhao and C. F. Pan, *Nanoscale*, 2016, **8**, 8078–8082.
37 Z. L. Wang, H. Y. Zhang, H. W. Cao, L. C. Wang, Z. Y. Wan, Y. F. Hao and X. T. Wang, *Int. J. Hydrogen Energy*, 2017, **42**, 17394–17402.
38 M. Y. Zhang, H. L. Lin, J. Cao, X. M. Guo and S. F. Chen, *Chem. Eng. J.*, 2017, **321**, 484–494.